

Temperature sensitivity and electrical stability of Sb/Mn co-doped SnO₂ ceramics

Guoxiang Jiang

Central South University

Zhicheng Li

Central South University

Chang You

Central South University

Wenbin Hao

Central South University

Zhiyuan Ma

Southwest Petroleum University

Hong Zhang (✉ hzhang@csu.edu.cn)

Central South University <https://orcid.org/0000-0003-3741-834X>

Research Article

Keywords: SnO₂, Sb/Mn co-doping, NTC thermistor, Electrical property, Aging characteristic

Posted Date: March 25th, 2021

DOI: <https://doi.org/10.21203/rs.3.rs-349472/v1>

License: © ⓘ This work is licensed under a Creative Commons Attribution 4.0 International License.

[Read Full License](#)

Abstract

SnO₂-based ceramics (Sn_{1-x}Sb_xO₂, 0 ≤ x ≤ 0.06, denoted as xATO; Sn_{0.95-y}Sb_{0.05}Mn_yO₂, 0 ≤ y ≤ 0.05, denoted as yMATO) for negative temperature coefficient (NTC) thermistors were prepared by solid state reaction method. XRD analysis revealed that all ceramics contain rutile-type crystalline structure and no impurity was detected. The effect of Sb- and Mn-doping on temperature sensitivity and electrical stability of the ceramic was investigated. The Sb-doped SnO₂ ceramics show high conductivity but lower temperature sensitivity for NTC thermistor. yMATO ceramics show typical NTC behavior contributed from both grain and grain-boundary effect. The room temperature resistivity from 3.88 Ω·cm to 38.5 kΩ·cm and temperature sensitivity constants ($B_{25/85}$) from 288 K to 5808 K can be adjusted by altering the content of Mn-ions. Mn-doping can enhance the electrical stability of the ceramics, the aging induced resistivity change rate is 0.6 % of 0.04MATO ceramic after being aged at 150 °C for 500 h, while 0.05ATO ceramic without Mn-doping has resistance change rate of -14.29 %.

1 Introduction

Due to the unique performance like high sensitivity, fast response and low cost, negative temperature coefficient (NTC) thermistors are playing important role in industrial and domestic aspects such as temperature sensing, temperature compensation, circuit protection, infrared detection, infrared imaging, and so on [1–4]. The most commonly used NTC thermistors are spinel-type transition metal oxides with general formula like AB₂O₄, such as Mn-Ni-O, Mn-Fe-O, Mn-Co-Ni-O, Mn-Co-Fe-Ni-O and Mn-Ni-Co-Cu-Zn-O systems, *etc.* [5–10]. In practice, the electrical properties of NTC thermistors are generally characterized by room temperature resistivity (ρ_{25}) and temperature sensitivity constant (B value). Controllable ρ_{25} and B values are required for diverse products in practical applications.

In the meanwhile, the electrical stability of NTC thermistors is also one of the key properties for practical applications. Nowadays, investigations on aging characteristics are mainly focused on spinel oxides, in which the adding induced resistance change was generally considered to be the rearrangement and/or redox reaction of the cations. Battault *et al.* pointed out that the aging origin in Mn_{3-x}Fe_xO₄ (0 ≤ x ≤ 1.51) thermistors was closely related to the migration and rearrangement of Fe³⁺ and Mn²⁺ ions between tetrahedral and octahedral sites in spinel structure [11]. Groen *et al.* found that oxidation reaction occurred at grain boundaries and the resulting cationic vacancies migration from grain boundaries to grains during aging process was responsible for aging deterioration in Mn-Ni-Fe-O system [12]. Furthermore, the poor sinterability of ceramics, ion oxidation and the reconfiguration of electrode/ceramic interface may also result in aging deterioration [13–15]. Several strategies have been employed to improve the electrical stability of the thermistors. Li *et al.* fabricated Mn_{1.95-x}Co_{0.21}Ni_{0.84}Na_xO₄ thermistors with excellent stability for that the second phase Na_{0.7}MnO_{2.05} can block the transport of oxygen vacancies [16]. Guan *et al.* reported that Fe doping can improve the electrical stability of LaCrO₃, with the resistance shifts less than 0.65 % [17].

Recent years, NTC thermistors based on single cation oxides such as SnO₂, ZnO, CuO and NiO, *etc.*, have attracted attentions [18–21]. Those single cation oxides have unique advantage that ρ_{25} and B value can be effectively adjusted by suitable ionic doping. For example, Yang *et al.* reported a thermo-sensitive NiO-based ceramic, ρ_{25} from 47 $\Omega\cdot\text{cm}$ to 1 M $\Omega\cdot\text{cm}$ and $B_{25/85}$ values from 2582 K to 8019 K were obtained by modifying the concentration of B³⁺ and Na⁺ ions [21]. Some works based on SnO₂-based ceramics have been reported, *e.g.*, Sb-doped SnO₂ oxides modified by Zr-, Ti-, Fe-, or Cr- ions, all of those showed excellent NTC characteristics [18, 22–24].

Despite of high adjustability of ρ_{25} and B value, the demand for high electrical stability is increasing. However, there has been little detailed work on the electrical stability of NTC thermistors based on those single cation oxides. In this work, Sb-doped SnO₂ ceramics modified by Mn-ion were prepared for NTC thermistors. The results show that the Sb/Mn co-doped SnO₂ NTC thermistors have controllable ρ_{25} and B value, and high electrical stability can be received with appropriate content of Mn-ions.

2 Experimental

Sb/Mn co-doped SnO₂ ceramics with nominal formula of Sn_{1-x-y}Sb_xMn_yO₂ ($x = 0, 0.01, 0.03, 0.05$ and 0.06 , denoted as $x\text{ATO}$; $y = 0, 0.01, 0.02, 0.03, 0.04, 0.045$ and 0.05 , denoted as $y\text{MATO}$) were synthesized by solid state reaction method. The raw materials are tin oxide (SnO₂, Xilong Scientific, China), antimony oxide (Sb₂O₃, Xilong Scientific, China) and manganese dioxide (MnO₂, Hengxing chemical reagent manufacturing, China). Appropriate amount of the raw materials was weighted according to the nominal formula of Sn_{1-x-y}Sb_xMn_yO₂, and were mixed by ball-milling for 1 hour in deionized water. The mixed slurries were dried at 110 °C for 12 h. Then the dried mixtures were calcined at 900 °C for 5 h in air. For each batch, 2 % (weight ratio) of CuO (Xilong Scientific, China) was added as the sintering aid in the calcined powders. The mixture was granulated with polyvinyl alcohol (PVA) solution, and then was pressed into pellets with a diameter of 12 mm and thickness of about 3 mm. The green pellets were sintered at 1250 °C for 1 h in air for the $y\text{MATO}$ samples, while, the samples without Mn dopant were sintered at 1300 °C for 1 h in air. For electrical property measurement, two opposite surfaces of as-sintered ceramics were polished and were brushed with silver paste. The silver coating was subsequently cured at 600 °C for 5 min to formed ohmic electrodes.

The phase composition and lattice parameters of the as-sintered ceramics were characterized by using X-ray diffractometer (XRD, Rigaku D/Max 2500, Japan) with Cu K_α radiation ($\lambda = 0.154056$ nm) in diffract angle (2θ) range between 10° and 90° at a scanning rate of 8 °·min⁻¹. For microstructure observation, the as-sintered ceramics were broken into pieces, and the morphology of fracture surfaces was observed using a scanning electron microscopy (SEM, JEOL JSM 7900F). Energy dispersive X-ray spectroscopy (EDS, Oxford Ultim Max 65) attached to the SEM was employed to analyze the elemental distributions in ceramics. X-ray photoelectron spectroscopy (XPS, K-alpha 1063, UK) was used for detecting the valence states of cations in ceramics. The densities of all ceramics were obtained by the Archimedes method in water, the relative density was calculated from the ratio between measured density and theoretical

density of the ceramics, i.e. $D_r = D_m/D_l$, where D_r is relative density, D_m is measured density, D_l is lattice density.

Resistance-temperature data (R - T) of the specimens were recorded by using a resistance-temperature measurement system (ZWC-C, Huazhong University of Science and Technology, China) under direct current (DC) condition in temperature range from 25 to 250 °C. The resistivity (ρ) was calculated based on the measured resistance (R) according to the equation of $\rho = R(S/h)$, where S and h are respectively electrode area (cm^2) and thickness (cm) of the measured sample. Alternating current (AC) impedance measurement were carried out by using an electrochemical measurement system (Gamry Reference 600, USA) in a frequency range from 1 Hz to 1 MHz, and the impedance data were analyzed by Gamry Echem Analyst program.

For investigation of electrical stability, aging treatment was conducted at 150 °C in air by putting the samples with ohmic electrodes in an oven. After being aged for 50 hours, the samples were taken out from the oven, and were put in an ambient temperature (25 °C) room for more than 1 h before the resistance measurement. After resistance measurement, the samples were placed back into oven for further ageing treatment. This process was repeated ten times and the aging duration was accumulated to 500 h. The resistance change rate is given by $\Delta R/R_0 = (R_i - R_0)/R_0$, in which R_0 is resistance measured at 25 °C before ageing treatment, R_i is resistance measured at 25 °C after each stage aging treatment.

3 Results And Discussion

3.1 Phase and microstructure

Figure 1 shows the XRD patterns of the as-sintered $\text{Sn}_{1-x-y}\text{Sb}_x\text{Mn}_y\text{O}_2$ ceramics with various contents of Sb- and Mn- dopants. All the diffraction peaks can be assigned to tetragonal rutile structure with a space group of $P4_2/mnm$ (136) (referred by PDF No. 41-1445, $a = b = 0.4738$ nm, $c = 0.3187$ nm). No impurity peak was detected. These indicate that Mn-, Sb- and Cu- ions have substituted into the SnO_2 lattice, or the content of impurity phase is too small to be detected.

Refined by Jade 6.0 + pdf2004 program, the lattice parameters for the prepared ceramics are listed in Table 1. The lattice parameters of 0ATO ceramic ($a = 0.4731$ nm, $c = 0.3182$ nm) are slightly smaller than those referred to the PDF no. 41-1445. It may result from the formation of oxygen vacancies for insufficient oxygen in the sintering environment and for the introduction of CuO that substitutes into the ATO lattice and produce oxygen vacancies. The lattice parameters of 0.05ATO ceramic are smaller than that of 0ATO. During the calcining and sintering processes, Sb^{3+} ion could be oxidized to Sb^{5+} ion. The ionic radius of Sb^{5+} (0.061 nm) is smaller than those of Sn^{4+} ion (0.069 nm) and Cu^{2+} (0.073 nm), resulting in decrease of lattice parameters.

Table 1
Lattice parameters, measured densities D_m , lattice densities D_l and relative densities D_r of the as-sintered $\text{Sn}_{1-x-y}\text{Sb}_x\text{Mn}_y\text{O}_2$ ceramics with different contents of Sb- and Mn- ions

Sample	$a = b$ (nm)	c (nm)	D_m ($\text{g}\cdot\text{cm}^{-3}$)	D_l ($\text{g}\cdot\text{cm}^{-3}$)	D_r (%)
0ATO	0.4731	0.3182	6.232	7.030	88.60%
0.05ATO	0.4727	0.3181	6.7259	7.051	95.4%
0.02MATO	0.4729	0.3180	6.5332	6.988	93.5%
0.04MATO	0.4728	0.3179	6.5508	6.934	94.5%

When Mn-ion was introduced into Sb-doped SnO_2 compounds, the related c lattice parameters decreased slightly with the rise of Mn-ion concentrations. The Mn-ions may have Mn^{2+} (0.066 nm), Mn^{3+} (0.058 nm) and Mn^{4+} (0.053 nm) ions, which can be confirmed by later XPS analysis. The ionic radii of most Mn-ions are smaller than those of Sn^{4+} , Sb^{5+} , Sb^{3+} and Cu^{2+} ions, leading to c lattice parameters decrease in y MATO ceramics.

SEM images of the as-sintered ceramics of 0ATO, 0.05ATO, 0.02MATO and 0.04MATO are shown in Fig. 2. As shown in Fig. 2a, the 0ATO ceramic show inhomogeneous particle size and some small pores. For the 0.05ATO ceramic, as shown in Fig. 2b, the average grain size is about 1–2 μm , and the grains contacted each other tightly. Figures 2c and 2d show that the grain sizes slightly increased with the increase of Mn-content in Mn-doped ATO ceramics.

Figure 3a is a secondary electron SEM image of a 0.04MATO ceramic. Elemental distributions of the area in Fig. 3a are shown in Figs. 3b – 3e. The results show that homogeneous elemental distribution of Sn, Sb, Mn and O exist in 0.04MATO ceramic.

The relative densities of 0ATO, 0.05ATO, 0.02MATO and 0.04MATO ceramics were measured by Archimedes displacement method, and were calculated by comparing the measured density D_m to lattice density D_l . The lattice density of each ceramic can be calculated by $D_l = MZ/N_A V$, where M is molecular weight, Z is number of atoms per unit cell ($Z = 2$ for SnO_2), N_A is the Avogadro constant and V is volume of unit cell ($V = a^2 c$ for SnO_2). The results are shown in Table 1. The Sb/Mn co-doped SnO_2 ceramics have high relative densities of 95.4 % (0.05ATO), 93.5 % (0.02MATO) and 94.5 % (0.04MATO).

3.2 Electrical properties

The relationship between logarithm of resistivity ($\ln\rho$) and reciprocal of absolute temperature ($1000/T$) for x ATO ceramics are shown in Fig. 4. One can see that all samples display nearly linear $\ln\rho$ - $1000/T$ relationship in the testing temperature range. The $\ln\rho$ - $1000/T$ relationship can be expressed by the Arrhenius law as shown in Eq. (1).

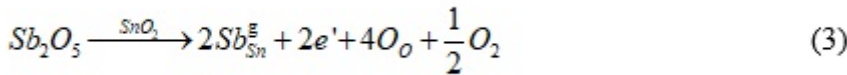
$$\rho = \rho_0 \exp\left(\frac{E_a}{kT}\right) = \rho_0 \exp\left(\frac{B}{T}\right) \quad (1)$$

where, ρ is resistivity at temperature T (in Kelvin), ρ_0 is a pre-exponential factor relating to the material characteristic, E_a is activation energy of conduction, k is the Boltzman constant. B is a material constant representing temperature sensitivity of a NTC thermistor. B value can be calculated by as Eq. (2).

$$B_{25/85} = \frac{\ln \rho_{25} - \ln \rho_{85}}{1/T_{25} - 1/T_{85}} \quad (2)$$

where, ρ_{25} and ρ_{85} are the resistances at temperature of 298 K (25 °C) and 358 K (85 °C), respectively. B value is written as $B_{25/85}$.

The 0ATO ceramic without Sb-dopant has a high room temperature resistivity (ρ_{25}) of 0.13 M Ω ·cm. Sb-doping reduced obviously the resistivity of SnO₂-based ceramics. ρ_{25} of x ATO ceramics are 9.41 Ω ·cm for $x = 0.01$, 6.09 Ω ·cm for $x = 0.03$, 3.88 Ω ·cm for $x = 0.05$ and 6.67 Ω ·cm for $x = 0.06$, respectively. These results are in agreement with the previous reports [23-24]. It is well known that SnO₂ is a semiconductor oxide. When the content of Sb₂O₃ is low, majority of Sb³⁺ ion could be oxidized to Sb⁵⁺ ion during calcining and sintering processes. Then Sb⁵⁺ ion acted as semiconductor donor and introduced weakly bound electrons (charge carriers) as shown in Eq. (3). The weakly bound electrons can be thermal activated and jump to conduction band from the donor level, leading to decrease of resistivity.



For each semiconductor, there is appropriate doping concentration to get the lowest resistivity. With further increase of Sb₂O₃ content, more Sb³⁺ ion were retained and acted as acceptors in SnO₂-based ceramic. As a result, the electron holes occurred and locate at the acceptor level near the valence band. Then the electron holes captured the weakly bound electrons that produced by Sb⁵⁺ ion, and decreased the concentration of weakly bound electrons, resulting in increase of resistivity.

The $B_{25/85}$ values of x ATO ceramics are 630, 505, 288 and 769 K for $x = 0.01, 0.03, 0.05$ and 0.06 , respectively. The low $B_{25/85}$ values mean that the x ATO ceramics themselves are not suitable for NTC thermistor application. In order to improve the temperature sensitivity, various contents of MnO₂ was introduced into Sn_{0.95}Sb_{0.05}O₂ ceramic in this work. The temperature dependence of resistivity in Arrhenius plot of y MATO ceramics with various contents of Mn-ions are shown in Fig. 5a. ρ_{25} and $B_{25/85}$ of y MATO ceramics as function of Mn- concentration are shown in Fig. 5b. It can be observed that Mn-

modified ATO ceramics show typical NTC characteristic. ρ_{25} and $B_{25/85}$ increased monotonically with the increase of Mn-ion content. For y is equal to 0.01, 0.02, 0.03, 0.04, 0.045 and 0.05, ρ_{25} are 0.053, 1.57, 12.9, 20.8, 26.5 and 38.5 k Ω ·cm respectively, and $B_{25/85}$ values are 1537, 3253, 4507, 5252, 5682 and 5808 K respectively. The adjustable ρ_{25} and $B_{25/85}$ values of y MATO system may meet various requirements in practical application.

As previous reports on the NTC thermistors based on single cation oxides [18–21], besides the band conduction contributed by donor or acceptor doping, polaron hopping is also one of the important conduction modes. The Mn-free ATO ceramics display high conductivity for donor doping of Sb^{5+} ion as shown in Eq. (3). The primary charge carriers in x ATO are weakly bound electrons, and the main conduction mode in x ATO should be the band conduction. When Mn-ion substituted into the ATO lattice, the electrons at donor level are not only thermally activated to conduction level for electrical conductivity, but also can be weakly bounded by Mn-ions followed by formation of Mn^{3+} and Mn^{2+} ions. For different valent cations exist at the Sn-sites in ATO, polaron hopping such as $\text{Mn}^{4+} \leftrightarrow \text{Mn}^{3+} \leftrightarrow \text{Mn}^{2+}$ may take place to contribute to the hopping conduction. The polaron hopping must overcome the lattice barriers, leading to high activation energy of conduction and high B values. In the meanwhile, the concentration of the electron charge carriers decreased with the increase of Mn-ion content, resulting in the increase of ρ_{25} .

3.3 AC impedance analysis

Complex impedance spectrum (CIS) is employed to characterize the electrical properties. Generally, an ideal CIS consists of three semicircles, which are associated with grain effect, grain boundary effect and electrode polarization effect, respectively. Figure 6 shows the Nyquist plots of y MATO ceramics measured at room temperature. Each CIS looks like to be composed of only one arc. An equivalent circuit $R_0(R_g - CPE_g)(R_{gb} - CPE_{gb})$ (as shown in the inset in Fig. 6b) was utilized to fit the measured impedance data. Here, R_0 , R_g and R_{gb} represent electrode contact resistance, grain resistance and grain boundary resistance, respectively. CPE is a constant phase element which used to replace the capacitor to accommodate the non-ideal Debye behavior. The capacitance (C) of each part can be calculated by the fitted resistance and CPE , i.e., $C = Q^{1/n} R^{(1-n)/n}$, where, Q is CPE parameter, n is a variable value related to the deviation from ideal Debye behavior, $n = 0$ for ideal resistor, $n = 1$ for ideal capacitor [25]. In Fig. 6, the measured data are marked by scattered symbolic points, and the curves are fitted results by equivalent circuit. The fitting curves are in good agreement with the measured data. The relevant fitted results are also listed in Table 2. One can get that the grain effect and grain boundary effect co-contribute to the electrical properties.

Table 2
 CIS fitted results of y MATO ceramics modified with various contents of Mn-ions, grain resistance (R_g), grain capacitance (C_g), grain boundary resistance (R_{gb}) and grain boundary capacitance (C_{gb})

Sample	R_g (Ω)	C_g (nF)	R_{gb} (Ω)	C_{gb} (nF)
$y = 0.01$	4.1	0.16	10.9	19.8
$y = 0.02$	183.3	1.76	350.2	5.91
$y = 0.03$	319.7	3.15	742.2	9.83
$y = 0.04$	3838	2.86	5519	8.79
$y = 0.045$	4918	3.60	5745	13.00
$y = 0.05$	7631	2.60	4721	27.20

3.4 Aging behavior

The plots of aging time dependence of resistance change rates ($\Delta R/R_0$) of y MATO ceramics ($y = 0, 0.01, 0.02, 0.03, 0.04, 0.045$ and 0.05) are shown in Fig. 7. In the initial aging stage (about 50 h), all samples show negative resistance change rate, *i.e.*, resistance decreased after aging 50 h. Then, 0MATO ceramic became stable. The 0MATO ceramic has final $\Delta R/R_0$ value of -14.29 % after aging for 500 h. While, the resistances of y MATO ceramics ($y > 0$) increased in aging time from 50 to 200 h and the $\Delta R/R_0$ values are positive. After 200 h aging treatment, all samples (except the 0.05MATO) became gradually stable. The 0.04MATO ceramic has the lowest resistance change rates ($\Delta R/R_0$) of 0.6 % after 500 h aging.

To investigate the possible aging behavior, the valence states of Sb and Mn elements in y MATO ceramics ($y = 0$ and 0.04) were analyzed by XPS before and after aging. The fitted XPS spectra before aging and after 500 h aging are shown in Fig. 8. The C 1s peak located at 284.8 eV acts as a reference for binding energy calibration of the XPS analysis. In Figs. 8a and 8b, Sb 3d_{3/2} can be convoluted into two peaks, the binding energy peaks locate at 539.2-539.4 eV and 539.9-540.1 eV. The two peaks can be attributed to Sb³⁺ and Sb⁵⁺ states [26], respectively. In Fig. 8c, the peaks locating at 639.8-639.9 eV, 640.9-640.8 eV and 642.0-642.1 eV were assigned to reflect from Mn²⁺, Mn³⁺ and Mn⁴⁺, respectively [27].

For $y = 0$ (0.05ATO without Mn-doping) ceramic, as shown in Fig. 8a, the ratio of ionic concentration of [Sb³⁺]/[Sb⁵⁺] was calculated to be 0.75 before aging. But the ratio decreased to 0.56 after aging. These indicate that the concentration of Sb³⁺ ion decreased during aging. So the origin of resistance decrease of 0.05ATO ceramic might be result from the oxidation reaction when the ceramics exposed in air for aging test. Generally, the surface of ceramic may adsorb oxygen molecules. According to the reports by Dai *et al.* [28], oxygen molecules (O₂) in atmospheric environment adhere to crystal surface, then may

capture electrons from ceramic surfaces and interfaces (also be grain boundaries) to turn into the adsorbed oxygen (O_{ad}^{n-} , $n \leq 2$). For the existence of oxygen vacancies inside grains and/or at grain boundaries in the ceramic, it is possible for O_{ad}^{n-} diffusing into the ceramic. As result, partial Sb^{3+} ion might be oxidized to Sb^{5+} ion. The increase of Sb^{5+} ionic concentration can induce more weakly bound electrons, resulting in the decrease of resistivity.

For 0.04MATO ceramic, as shown in Figs. 8b, the ration of ionic contents $[Sb^{3+}]/[Sb^{5+}]$ is 0.81 before aging, while the one is 0.72 after aging. The decrement in ionic ratios is smaller than that in 0.05ATO ceramic. On the other hand, as calculated from the XPS spectra as shown in Figs. 8c, the percentage of Mn^{2+} , Mn^{3+} and Mn^{4+} ions in the sample is 17.24%: 26.06%: 56.70% before aging, while the one became 4.69%, 21.78% and 73.53% after aging. Obviously, the content of Mn^{4+} ion increased, and the ones of Mn^{3+} and Mn^{2+} ions decreased. With the introduction of Mn ion in the ceramics, Mn^{3+} and Mn^{2+} ions were oxidized to higher valence state with aging. These processes would restrain the oxidation of Sb^{3+} ion and reduced the resistance change of samples during aging. At the same time, the decrease of Mn^{2+} and Mn^{3+} concentrations lead to the decrease of Mn^{2+}/Mn^{3+} and Mn^{3+}/Mn^{4+} ion pairs, and reduce the effective sites for hopping conduction model. Thus, resistances of Mn-doped ceramics increased at the aging period of 50 to 200 h. It concluded, the addition of MnO_2 could improve the electrical stability by suppressing the oxidation of Sb-ion.

4 Conclusions

A series of SnO_2 -based ceramics ($Sn_{1-x}Sb_xO_2$, $0 \leq x \leq 0.06$; $Sn_{0.95-y}Sb_{0.05}Mn_yO_2$, $0 \leq y \leq 0.05$) were successfully synthesized by conventional solid state reaction. All the ceramics have tetragonal rutile-type SnO_2 phase. Sb dopants can enhance the electrical conductivity of SnO_2 ceramic by orders of magnitude, but the $Sn_{1-x}Sb_xO_2$ ceramics shows lower temperature sensitivity. The $Sn_{0.95-y}Sb_{0.05}Mn_yO_2$ ceramics exhibit typical NTC characteristic, and room temperature resistivity ρ_{25} and temperature sensitivity $B_{25/85}$ are adjusted in a large range. The $Sn_{0.91}Sb_{0.05}Mn_{0.05}O_2$ ceramic show lowest resistance change rate of 0.6 % after being aged in air for 500 h, while $Sn_{0.95}Sb_{0.05}O_2$ ceramic has resistance change rate of -14.29 %. The aging induced resistance drift originated from the oxidation of Sb-ion. The appropriate amount of Mn-ion doping can restrain the conversion process from Sb^{3+} to Sb^{5+} and show more stable electrical property. The unique merit of controllable ρ_{25} and $B_{25/85}$ value as well as high electrical stability make the Sb/Mn co-doped SnO_2 ceramics suitable for NTC thermistors.

Declarations

Acknowledgments

This work is supported by research funds from the Hunan Wedid Materials Technology Co., Ltd., China (No. 738010241), the National Natural Science Foundation of China (No. 51767021) and Key Area Research and Development Program of Guangdong Province, China (No. 2019B090913002)

Declaration of Competing Interest

The authors declare that they have no known competing financial interests or personal relationships that could have appeared to influence the work reported in this paper.

References

- [1] A. Feteira, Negative temperature coefficient resistance (NTCR) ceramic thermistors: an industrial perspective. *J. Am. Ceram. Soc.* **92** (2009) 967-983.
- [2] A. Feteira, K. Reichmann, NTC ceramics: past, present and future. *Adv. Sci. Technol.* **67** (2010) 124-133.
- [3] P. Atanasijevic, P. Mihailovic, Temperature compensation of NTC thermistors based anemometer. *Sens. Actuator A-Phys.* **285** (2019) 210-215.
- [4] Y. Zhao, S.S. Berbano, L. Gao, K. Wang, J. Guo, K. Tsuji, J. Wang, C.A. Randall, Cold-sintered V_2O_5 -PEDOT: PSS nanocomposites for negative temperature coefficient materials. *J. Eur. Ceram. Soc.* **39** (2019) 1257-1262.
- [5] H. Gao, C. Ma, B. Sun, Preparation and characterization of $NiMn_2O_4$ negative temperature coefficient ceramics by solid-state coordination reaction. *J. Mater. Sci.-Mater. Electron.* **25** (2014) 3990–3995.
- [6] J. Guo, H. Zhang, Z. He, S. Li, Z. Li, Electrical properties and temperature sensitivity of Mo-modified $MnFe_2O_4$ ceramics for application of NTC thermistors. *J. Mater. Sci.-Mater. Electron.* **29** (2018) 2491–2499.
- [7] W. Kong, W. Wei, B. Gao, A. Chang, A study on the electrical properties of Mn-Co-Ni-O thin films grown by radio frequency magnetron sputtering with different thicknesses. *Appl. Surf. Sci.* **423** (2017) 1012-1018.
- [8] Q. Wang, W. Kong, J. Yao, A. Chang, Fabrication and electrical properties of the fast response $Mn_{1.2}Co_{1.5}Ni_{0.3}O_4$ miniature NTC chip thermistors. *Ceram. Int.* **45** (2019) 378-383.
- [9] H. Han, K.R. Park, Y. Hong, K. Shim, S. Mhin, Effect of Fe incorporation on cation distributions and hopping conduction in Ni-Mn-Co-O spinel oxides. *J. Alloys. Compd.* **732** (2018) 486-490.
- [10] K. Park, K.J. Lee, The effect of ZnO content and sintered temperature on the electrical properties of Cu-containing $Mn_{1.95-x}Ni_{0.45}Co_{0.15}Cu_{0.45}Zn_xO_4$ NTC thermistors. *J. Alloys. Compd.* **475** (2009) 513-517.
- [11] T. Battault, R. Legros, A. Rousset, Aging of iron manganite negative temperature coefficient thermistors. *J. Mater. Res.* **13** (1998) 1238-1242.

- [12] W.A. Groen, C. Metzmacher, V. Zaspalis, P. Huppertz, S. Schuurman, Aging of NTC ceramics in the system Mn-Ni-Fe-O. *J. Eur. Ceram. Soc.* **21** (2001) 1793-1796.
- [13] D. Li, S. Zhao, K. Xiong, H. Bao, C. Nan, Aging improvement in Cu-containing NTC ceramics prepared by co-precipitation method. *J. Alloys. Compd.* **582** (2014) 283-288.
- [14] Z. Wang, C. Zhao, P. Yang, L. Winnubst, C. Chen, Effect of annealing in O₂ or N₂ on the aging of Fe_{0.5}Mn_{1.84}Ni_{0.66}O₄ NTC ceramics. *Solid State Ionics.* **177** (2006) 2191-2194.
- [15] R. Metz, Electrical properties of NTC thermistors made of manganite ceramics of general spinel structure: Mn_{3-x-x'}M_xN_xO₄ (0 ≤ x+x' ≤ 1; M and N being Ni, Co or Cu). Aging phenomenon study. *J. Mater. Sci.* **35** (2000) 4705-4711.
- [16] H. Li, I.P.L. Thayil, X. Ma, X. Sang, H. Zhang, A. Chang, Electrical properties and aging behavior of Na-doped Mn_{1.95}Co_{0.21}Ni_{0.84}O₄ NTC ceramics. *Ceram. Int.* **46** (2020) 24365–24370.
- [17] F. Guan, Z. Dang, S. Huang, J. Wang, I. Milisavljevic, D. Carloni, X. Cheng, Y. Wu, LaCr_{1-x}Fe_xO₃ (0 ≤ x ≤ 0.7): a novel NTC ceramic with high stability. *J. Eur. Ceram. Soc.* **40** (2020) 5597-5601.
- [18] P. Ouyang, H. Zhang, Y. Zhang, J. Wang, Z. Li, Zr-substituted SnO₂-based NTC thermistors with wide application temperature range and high property stability. *J. Mater. Sci.-Mater. Electron.* **26** (2015) 6163-6169.
- [19] B. Yang, H. Zhang, J. Guo, Y. Liu, Z. Li, Electrical properties and thermal sensitivity of Ti/Y modified CuO-based ceramic thermistors. *Front. Mater. Sci.* **10** (2016) 413-421.
- [20] P. Li, H. Zhang, C. Gao, G. Jiang, Z. Li, Electrical property of Al/La/Cu modified ZnO-based negative temperature coefficient (NTC) ceramics with high ageing stability. *J. Mater. Sci.-Mater. Electron.* **30** (2019) 19598-19608.
- [21] Z. Yang, H. Zhang, Z. He, B. Li, Z. Li, Influence of B³⁺ and Na⁺ ions on electrical property and temperature sensitivity of NiO-based ceramics. *J. Mater. Sci.-Mater. Electron.* **30** (2019) 3088-3097.
- [22] Y. Zhang, Y. Wu, H. Zhang, W. Chen, G. Wang, Z. Li, Characterization of negative temperature coefficient of resistivity in (Sn_{1-x}Ti_x)_{0.95}Sb_{0.05}O₂ (x ≤ 0.1) ceramics. *J. Mater. Sci.-Mater. Electron.* **25** (2014) 5552-5559.
- [23] J. Zhang, H. Zhang, B. Yang, Y. Zhang, Z. Li, Temperature sensitivity of Fe-substituted SnO₂-based ceramics as negative temperature coefficient thermistors. *J. Mater. Sci.-Mater. Electron.* **27** (2016) 4935-4942.
- [24] W. Yan, H. Zhang, X. Wang, C. You, Z. Li, Characterization of electrical conductivity and temperature sensitivity of Cr/Sb-modified SnO₂ ceramics. *J. Mater. Sci.-Mater. Electron.* **31** (2020) 4040-4049.

[25] I. Ahmad, M.J. Akhtar, R.T.A. Khan, M.M. Hasan, Change of Mott variable range to small polaronic hole hopping conduction mechanism and formation of Schottky barriers in $\text{Nd}_{0.9}\text{Sr}_{0.1}\text{FeO}_3$. *J. Appl. Phys.* **114** (2013).

[26] M. Li, P. Cheng, G. Luo, J.M. Schoenung, Q. Shen, Effects of Sb oxidation state on the densification and electrical properties of antimony-doped tin oxide ceramics. *J. Mater. Sci.-Mater. Electron.* **26** (2015) 4015-4020.

[27] M.C. Biesinger, B.P. Payne, A.P. Grosvenor, L.W.M. Lau, A.R. Gerson, R.S.C Smart, Resolving surface chemical states in XPS analysis of first row transition metals, oxides and hydroxides: Cr, Mn, Fe, Co and Ni. *Appl. Surf. Sci.* **257** (2011) 2717-2730.

[28] W. Dai, X. Pan, C. Chen, S. Chen, W. Chen, H. Zhang, Z. Ye, Enhanced UV detection performance using a Cu-doped ZnO nanorod array film. *RSC. Adv.* **4** (2014) 31969-31972.

Figures

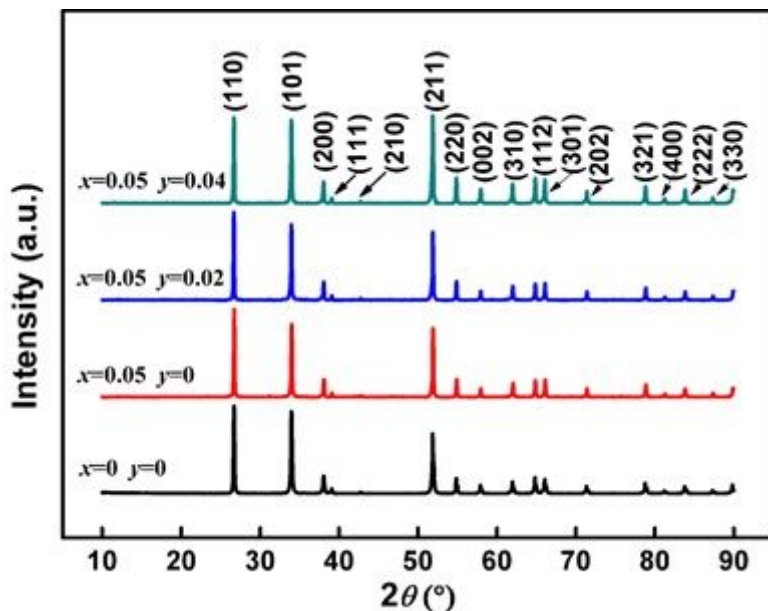


Figure 1

X-ray diffraction patterns of the as-sintered $\text{Sn}_{1-x-y}\text{Sb}_x\text{Mn}_y\text{O}_2$ ceramics

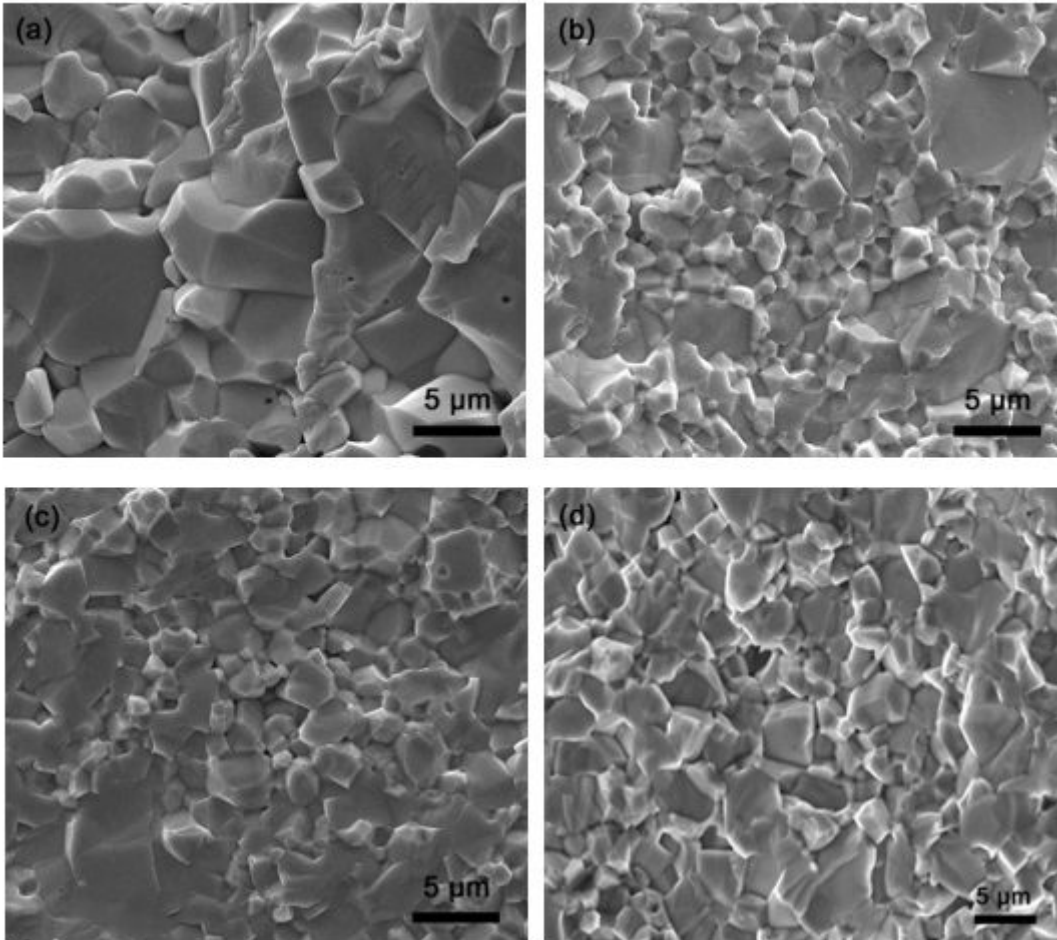


Figure 2

SEM images of cross sectional view of SnO₂-based ceramics, (a) 0ATO, (b) 0.05ATO, (c) 0.02MATO, (d) 0.04MATO

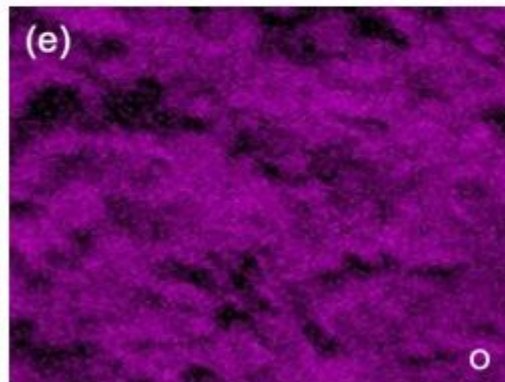
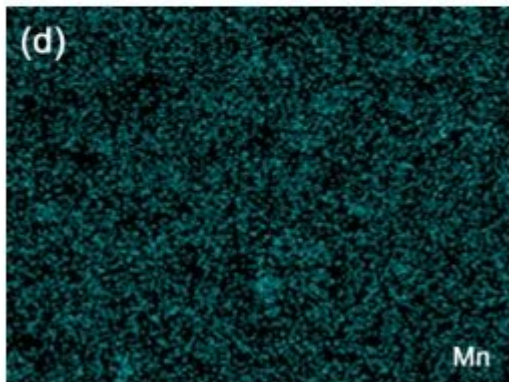
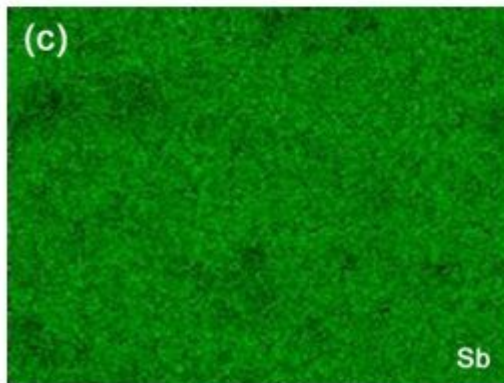
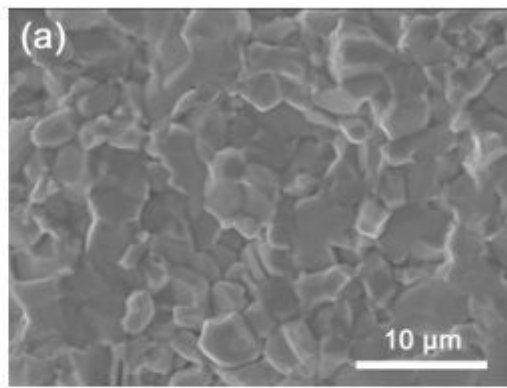


Figure 3

EDS analysis of elemental distribution in 0.04MATO ceramic, (a) secondary electron SEM image, (b) Sn element mapping, (c) Sb element mapping, (d) Mn element mapping, (e) O element mapping

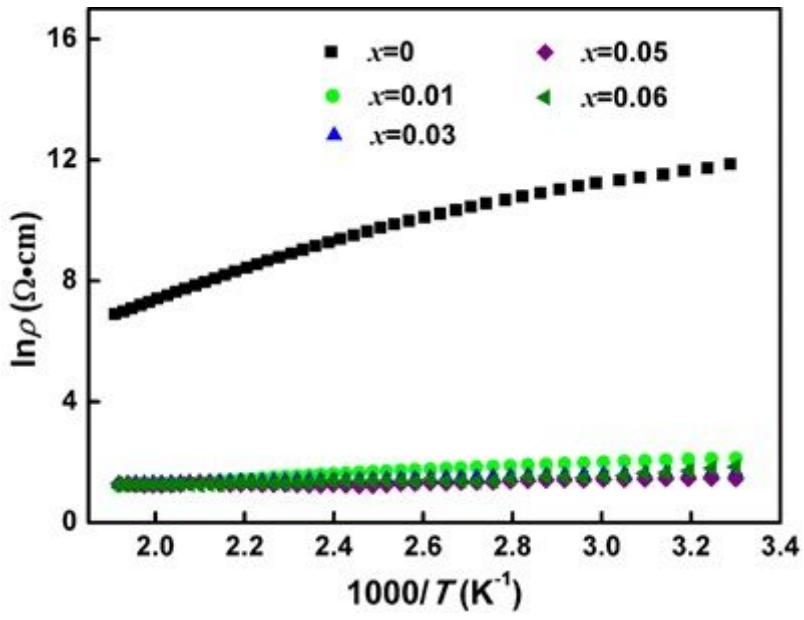


Figure 4

Electrical properties of xATO ceramics with various concentrations of Sb-ions

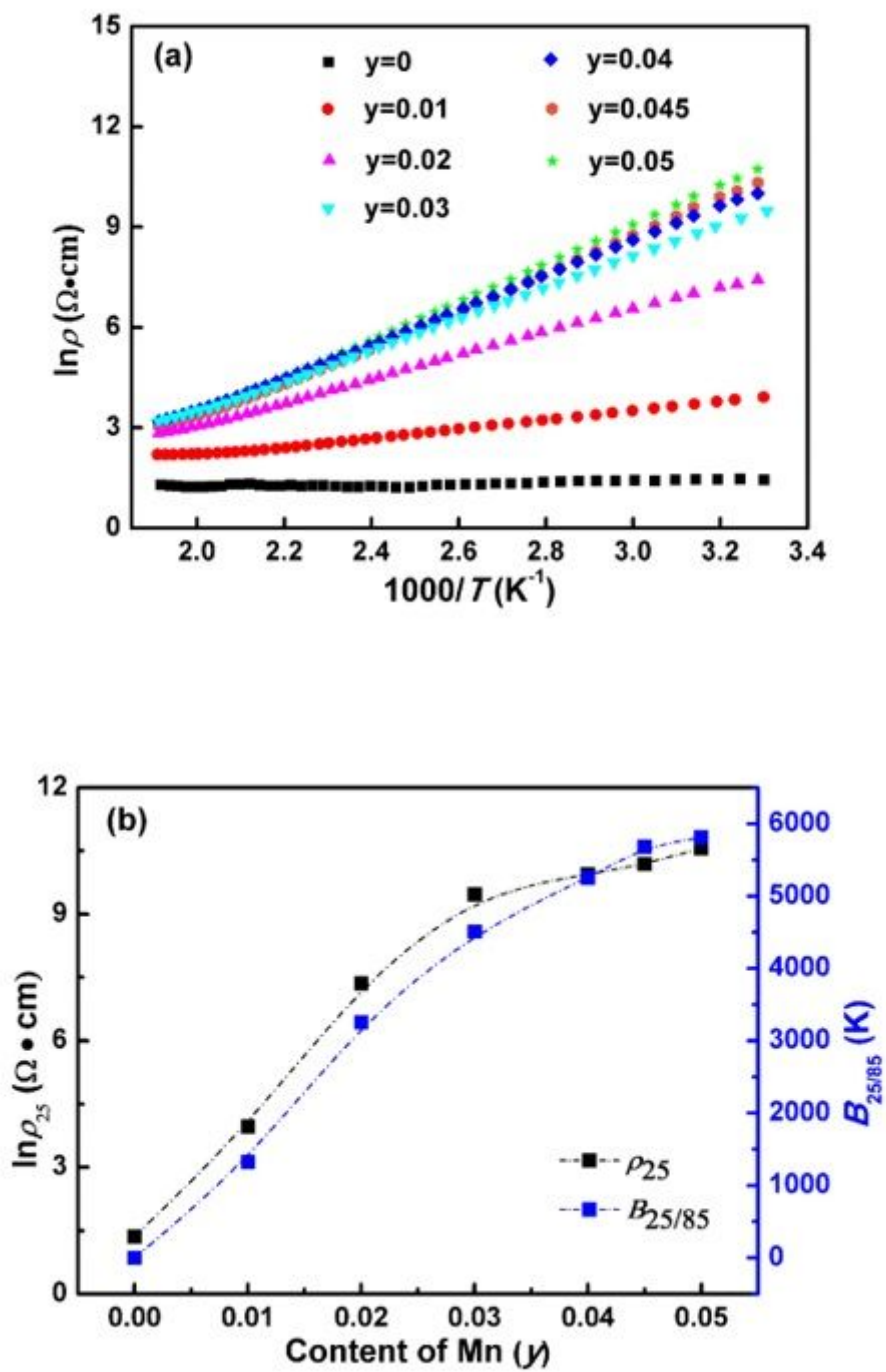


Figure 5

Electrical properties of the as-sintered yMATO ceramics, (a) plots of $\ln \rho$ - $1000/T$, (b) Mn concentration dependence of ρ_{25} and $B_{25/85}$

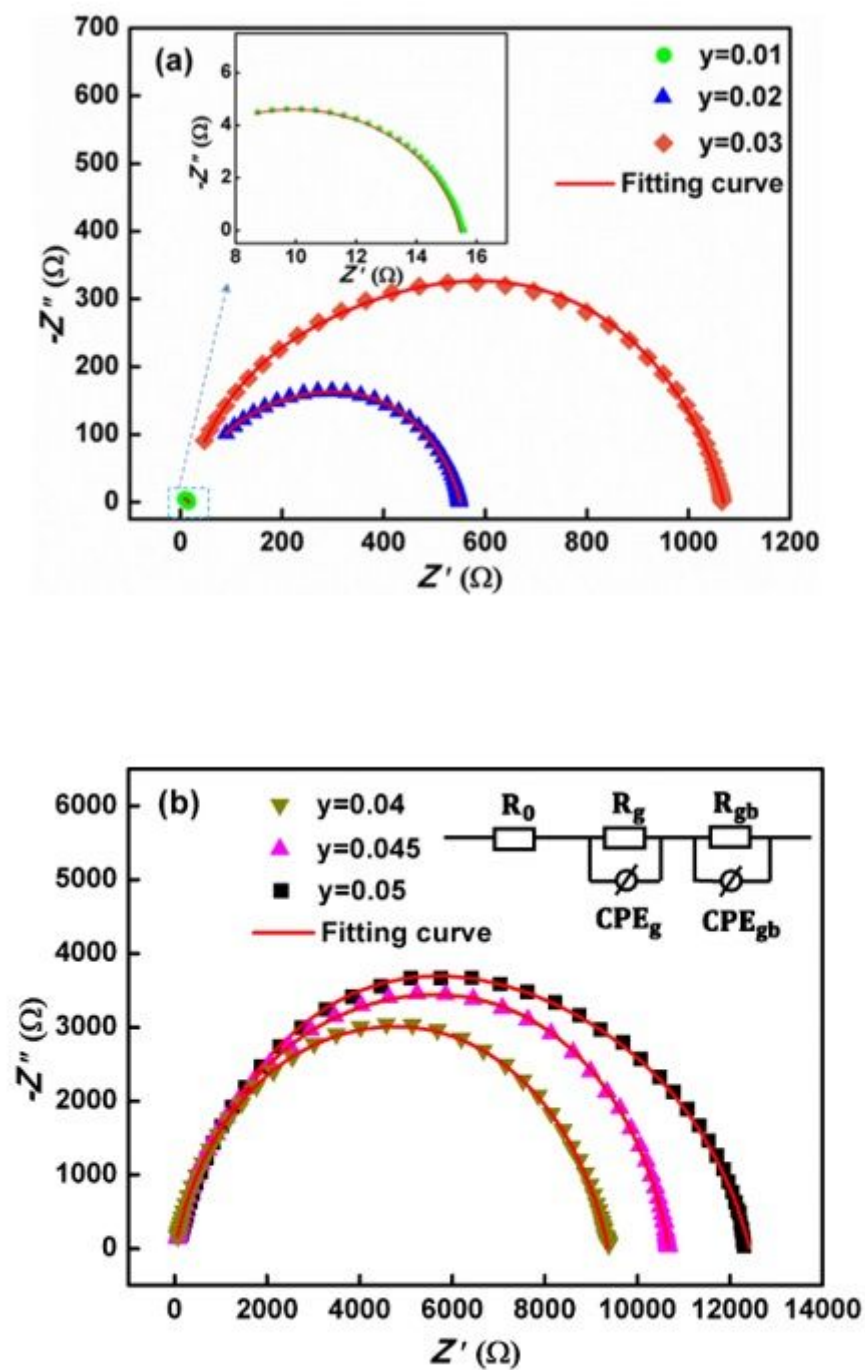


Figure 6

Nyquist plots of yMATO ceramics modified with various content of Mn-ions, measured at room temperature, (a) $y = 0.01, 0.02, 0.03$, (b) $y = 0.04, 0.045, 0.05$. The inset in Fig. 6b is an equivalent circuit for data fitting

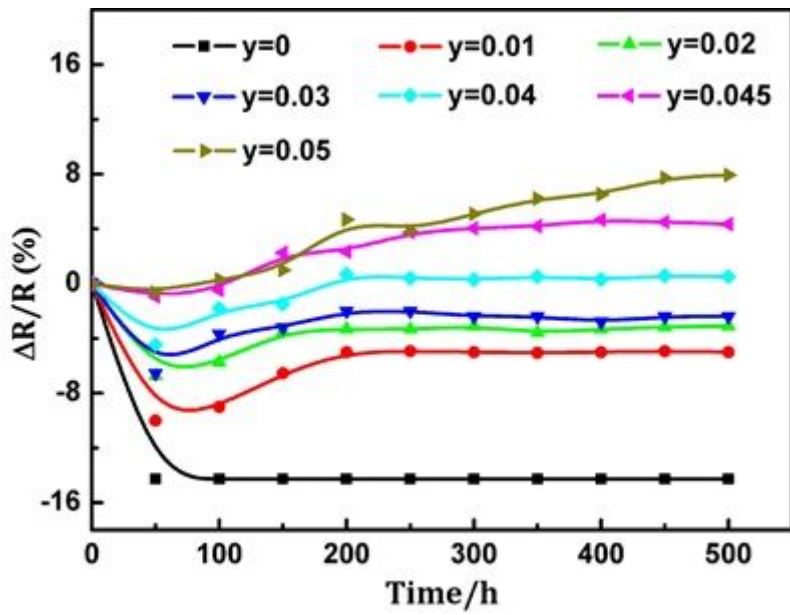


Figure 7

Effect of Mn content on the resistance change rate $\Delta R/R$ of $0.05\text{Sb}/y\text{Mn-SnO}_2$ ($y = 0, 0.01, 0.02, 0.03, 0.04, 0.045, 0.05$) ceramics during the aging process treated at $150\text{ }^\circ\text{C}$

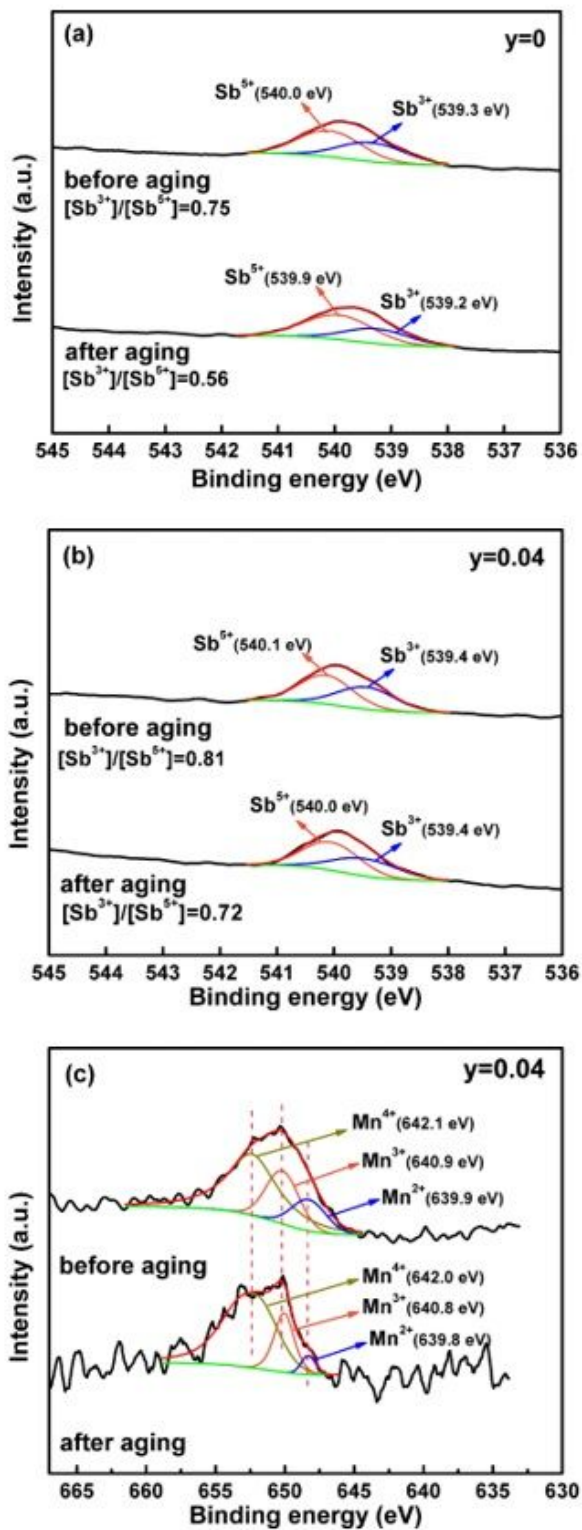


Figure 8

XPS analysis of y MATO ($y = 0, 0.04$) ceramics before aging and after being aged for 500 h, (a) Sb 3d_{3/2} spectra for $y = 0$, (b) Sb 3d_{3/2} spectra for $y = 0.04$, (c) Mn 2p spectra for $y = 0.04$